Comparison of pass-by railway noise indicators obtained from standard engineering methods with measured values

Julien Maillard, Dirk Van-Maercke, Franck Poisson, Jean-Philippe Regairaz, Jean-Benoît Dufour

Comparison of pass-by railway noise indicators obtained from standard engineering methods with measured values.

J. Maillard[1] D. Van-Maercke[1] F. Poisson[2] J.-P. Regairaz[3] J.-B. Dufour[4]

[1] Centre Scientifique et Technique du Bâtiment (CSTB),
24 rue Joseph Fourier, 38400 Saint Martin D'Hères, France
[2] SNCF-Mobilités, Agence d'Essai Ferroviaire,
21, avenue du Président Salvador Allende, 94407 Vitry Sur Seine Cedex, France
[3] SNCF-Réseau Direction Générale Industrielle & Ingénierie,
6, avenue François Mitterrand, 93574 La Plaine Saint Denis Cedex, France
[4] Geomod, 89 rue de la Villette, 69003 Lyon, France
julien.maillard@cstb.fr

ABSTRACT

Long-term averaged noise indicators are commonly used for designing and sizing protections, and to satisfy existing regulations for railway infrastructures. These long-term indicators allow to assess the exposure of populations to environmental noise and, in turn, evaluate health related effects. However, long-term indicators may not correlate well with noise perception by residents. In case of high-speed train pass-by, for example, short-term indicators are more directly linked to the high variation of noise level during a short event. For rolling stock characterization, indicators such as $L_{Aeq,Tp}$, SEL, TEL and $L_{A,max}$ are commonly used during the design phase and the validation of the rolling stock. As an extension, such indicators, including $L_{Aeq,Te}$, may also be used to assess the noise perceived by residents for single pass-by events. In this context, a new calculation scheme, compatible with existing normative methods in France and Europe, has been developed for predicting event-related noise indicators in complex environments, under varying meteorological conditions. The standard prediction methods are adapted to obtain the time-dependent sound pressure level during the train pass-by and then derive the different short-term indicators. This paper presents a validation study comparing measured and calculated short term indicators according to current engineering methods. Results are given for different trains and speeds as well as different sites and receiver configurations.

1. INTRODUCTION

Railway transportation represents a better alternative to road transportation in terms of environmental impact. However, it remains today a significant source of noise pollution. As a result, the acceptability of railway infrastructures by residents living nearby becomes a key issue for a successful transition to increased railway traffic. Existing regulations in France impose noise limits in terms of long-term averaged noise levels. The main objective of these regulations is to reduce long-term exposure and in turn, health-related effects [1], [2]. Acceptability, on the other hand, depends on the perception of railway noise by residents. The perception can be evaluated directly using questionnaires, in-situ or in controlled laboratory environments [3], or predicted using appropriate models. Today, the prediction of noise perception based on acoustical and psychoacoustical indices is still a very active research field and much progress remains to be made [4], [5]. Long term indicators are well correlated with annoyance. Short term indicators such as $L_{A,max}$ can be used to describe short term annoyance but there is no significant improvement compared to L_{Aeq} [6]. Previous works have already shown, though, that short-term noise indicators better correlate to sleep disturbance [7]. Therefore, the prediction of short-term indicators remains important to help railway operators and infrastructure managers evaluate at design stage the effect of mitigation measures on noise perception.

The objective of the work presented in this paper is to propose a practical approach for obtaining event-related noise indicators based on existing engineering methods [8], [9], [10] commonly implemented in sound mapping software tools. It is applied here to the case of railway noise. The existing propagation methods are adapted to first obtain the time-dependent sound pressure level during the train pass-by. Different short-term indicators such as $L_{Aeq,Tp}$, SEL, TEL and $L_{A,max}$ can then be derived from the pass-by level signature [11]. This paper presents a preliminary validation of the proposed approach for which calculated short-term indicators are compared with measured values for several configurations of train pass-by.

The outline of the paper is as follows. First, the calculation approach is briefly presented. Then the measurement site and associated model are described. Finally, the measured $L_{Aeq,Tp}$ and $L_{A,max}$ levels are compared to the calculated values obtained from the model.

2. APPROACH

The approach uses the existing standards for outdoor noise propagation and noise emission of ground transportation [8], [9], [10]. These methods are based on the calculation of acoustic attenuations in multiple

frequency bands for each propagation path detected between a source and a receiver. The path detection is implemented in a first stage using methods from geometrical acoustics such as ray tracing or the image source method. For road and railway infrastructures, the propagation paths are defined between elementary sections of line sources. The sections should be short enough such that the acoustic attenuation to the receiver can be considered constant over the length of the source section.

In standard noise mapping, for each propagation path identified during the geometric calculation, the attenuation spectrum is calculated using one of the standard methods. The spectrum is then added to the emission power of the associated source segment to obtain the contribution of the path to the receiver sound pressure level. The final result is obtained by summing over all propagation paths. For the calculation of short-term noise indicators, the approach proposed here relies on the calculation of the time dependent evolution of the sound pressure level at the receiver, during the motion of a source along the line source path. This is illustrated schematically in Figure 1. The principle of the approach is to convert the noise level contribution of each propagation path intersecting the line source over a segment (s_1, s_2) to a constant level in time between instants (t_1, t_2).

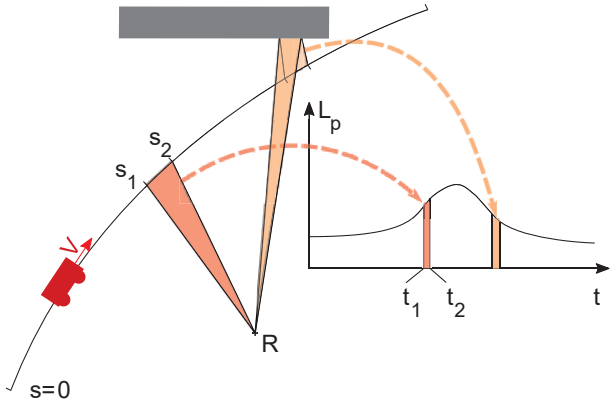

Figure 1: Calculation of the noise level time signature.

In more details, the approach involves the following steps. First perform the geometric calculation to detect propagation paths between source segments and receiver. For each propagation path, compute the acoustic attenuation according to one of the standard engineering methods. Store the path attenuation, the intersected source coordinates (s_1, s_2) and the propagation distances to the receiver (d_1, d_2). Then for each elementary source of a vehicle moving at speed V on the line source path, iterate over all stored propagation paths and calculate the instants (t_1, t_2) as:

$$t_i = s_i/V + d_i c, \qquad i = 1,2 \tag{1}$$

where c is the speed of sound. The effect of Doppler shift on the sound pressure level is introduced as a gain expressed in dB as:

$$G_{doppler} = -10N \log\left(\frac{t_2 - t_1}{V(s_2 - s_1)}\right) \tag{2}$$

where N depends on the physical source model [12] ($N = 2$ for the implementation used in this work). The source contribution over the period (t_1, t_2) is obtained by summing its emission power spectrum with the propagation path overall attenuation spectrum including the above Doppler shift gain. Note that geometrical spreading may be separated from the constant excess attenuation spectrum over (s_1, s_2) and evaluated individually at s_1 and s_2, yielding a piece wise linear evolution over (t_1, t_2). After summing all propagation path contributions from all vehicle elementary sources, the source noise level time signature is obtained and derived short-term indexes such as $L_{Aeq,Tp}$, SEL, TEL and $L_{A,max}$ may be calculated [11].

The proposed approach is implemented in MithraSIG©. To guaranty sufficient resolution in the time signature and improve accuracy, the calculation of short-term indexes as described above is preferably carried out using a small angular decomposition of line sources (one degree for the results presented below), resulting in non-overlapping elementary source segments over which the excess attenuation may be considered constant.

3. VALIDATION DATA

The proposed technique is validated against measured data obtained from a previous measurement campaign carried out by SNCF at two receiver locations near a high-speed train track on a mostly flat terrain. The track is equipped with UIC60 long welded rail, bi-bloc concrete sleepers, Pandrol Fastclip fasteners and 4.5mm thick rail pad. The two receivers are positioned at 25 and 150 m from the nearest track. A view of the site near the 25 m microphone is shown in Figure 2.

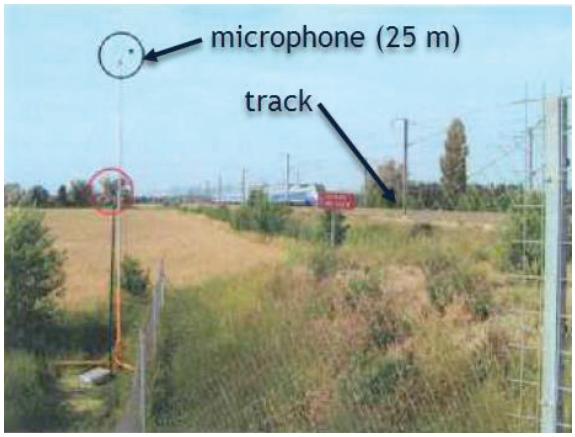

Figure 2: View of the measurement site near the 25 m microphone.

The track is on a 3 m embankment and the receivers placed 3.5 m above the rail head. Figure 3 shows a top view of the measurement site modelled in MithraSIG©.

All measurements were performed the same day. The train types measured on the track and their occurrence are listed in Table 1. The train speed was measured using two optical trigger sensors. Speed values range between 274 and 300 km/h.

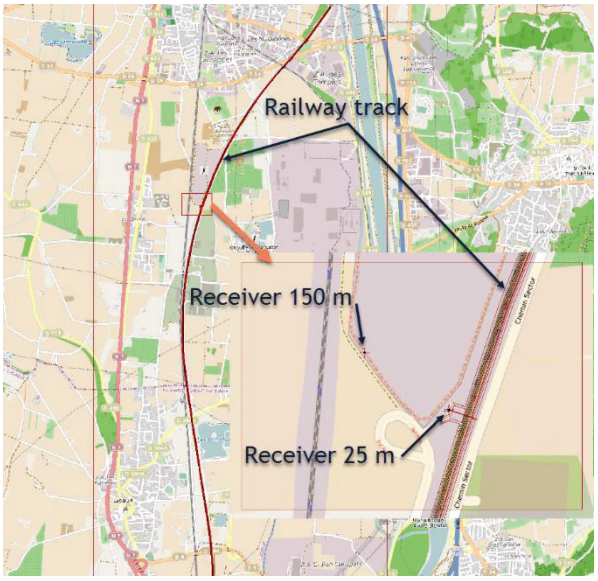

Figure 3: MithraSIG© model of the measurement site.

Train type (color legend)	*Length (m)*	*Number*
Single Unit TGV Réseau (**red**)	200	15
Single Unit TGV Duplex (**yellow**)	200	23
Multiple Unit TGV Réseau (**blue**)	400	3
Multiple Unit TGV Duplex (**cyan**)	400	9

Table 1: Measured train types, length and occurrence.

Figure 4 and Figure 5 present the measured $L_{Aeq,Tp}$ versus speed for the 25 m and 150 m receiver location, respectively, using the colors specified in Table 1.

Note that all measurement data is confidential. Thus, the absolute index values are not shown on the following figures. Each graduation on the y-axis of all figures presented in this paper represents a 2 dB increment.

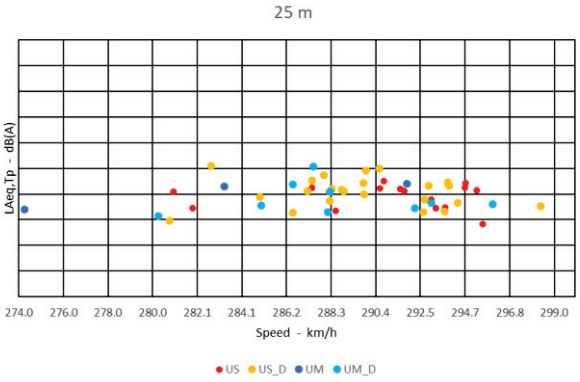

Figure 4: Measured $L_{Aeq,Tp}$ at 25 m (see Table 1 for legend).

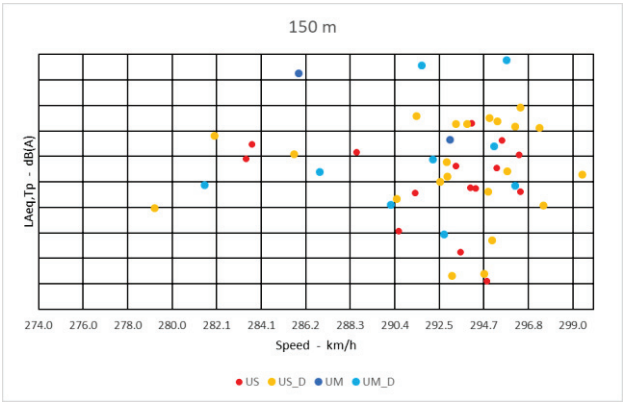

Figure 5: Measured $L_{Aeq,Tp}$ at 150 m (see Table 1 for legend).

Figure 6 and Figure 7 present the measured $L_{A,max,1sec}$ versus speed for the 25 m and 150 m receiver location, respectively. Note that the difference between the $L_{A,max}$ values and the $L_{Aeq,Tp}$ values for a given train is relatively small, around 2 dB(A). It is mainly due to the train composition. The main sources are located around each bogie and duplicated all along the train. The emergence of the other sources located on the power cars (pantograph, nose, …) is not sufficient to induce a big increase of the $L_{A,max}$ value.

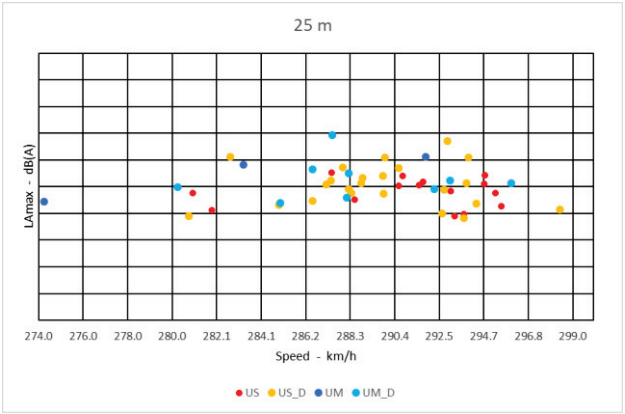

Figure 6: Measured $L_{A,max,1sec}$ at 25 m (see Table 1 for legend).

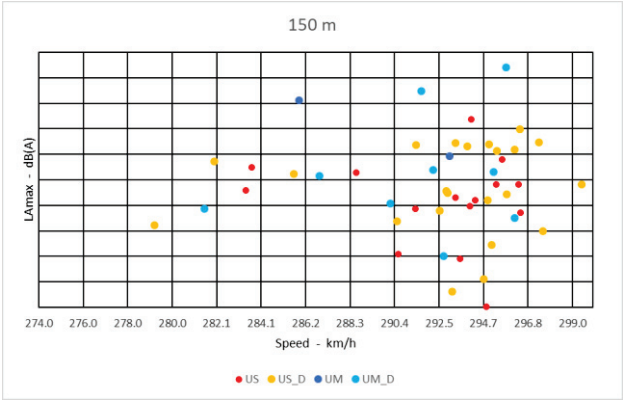

Figure 7: Measured $L_{A,max,1sec}$ at 150 m (see Table 1 for legend).

The measurement site is modeled in MithraSIG© to obtain for each train type the $L_{Aeq,Tp}$ and $L_{A,max}$ values over speed varying between 274 and 300 km/h with a 2 km/h

increment. The calculations use the French NMPB2008 method for the propagation [8] and SNCF railway data base for the train emission model (2012 version). This data base defines the position (height and distribution along the train units) and power spectrum model of the elementary noise sources representing the train. The power spectrum is defined in third-octave bands as:

$$L_W^j(V) = A\log(V/V_0) + L_{W,0}^j \qquad (3)$$

where j denotes the frequency band index and $L_{W,0}^j$ is the reference power spectrum at speed V_0. All calculations were carried out assuming favorable propagation conditions for the weather effects on the calculated attenuations. Ground type D (natural soil, fields or meadow) is chosen to match the type of ground of the measurement site.

Figure 8 shows the calculated signature and associated short-term indexes for the Multiple Unit TGV Duplex at 286 km/h for the 150 m receiver as presented in MithraSIG©. In the lower part of the figure, the frequency spectrum of the selected index (SEL) is also presented.

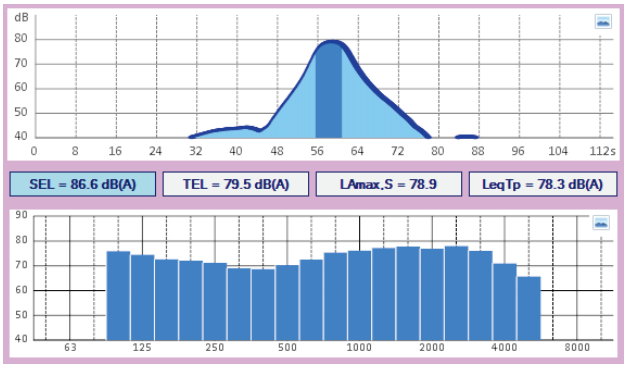

Figure 8: Signature, short-term indexes and SEL spectrum at 150 m for the Multiple Unit TGV Duplex at 286 km/h (MithraSIG©).

4. RESULTS

This section presents the comparison results of measured and calculated pass-by levels for the $L_{Aeq,Tp}$ and $L_{A,max}$ indexes.

The SNCF emission model does not differentiate between the TGV and TGV Duplex train types (see Table 1). Consequently, the comparison discussed below considers all Single Unit measurements (TGV and TGV Duplex combined) versus Single Unit calculations. The same type of comparison is then applied to Multiple Unit trains. In each case, the measured and calculated data is curved-fitted in the least square sense using a linear regression in $\log(V)$ to follow the noise emission model in Eq. (3). That is the estimated value $\hat{y}$ for $L_{Aeq,Tp}$ or $L_{A,max}$ versus speed V is expressed as

$$\hat{y} = Ax + B \qquad (4)$$

where $x = \log(V)$. The coefficients A and B are calculated according to:

$$A = \frac{\sum_i (y_i - \bar{y})(x_i - \bar{x})}{\sum_i (x_i - \bar{x})^2} \quad , \quad B = \bar{y} - A\bar{x} \qquad (5)$$

with $\bar{x}$, the x_i's mean value and $\bar{y}$, the y_i's mean value. The standard deviation for the linear regression is then obtained as:

$$\sigma = \sqrt{\frac{1}{N}\sum_i (y_i - \hat{y}_i)^2} \qquad (6)$$

The linear fit in $\log(V)$ is first performed on the measured values of $L_{Aeq,Tp}$ and $L_{A,max}$ (the y_i's). The procedure is then repeated on the calculated values for comparison purpose.

4.1 Measured and calculated $L_{Aeq,Tp}$

This section discusses the comparison results obtained for the $L_{Aeq,Tp}$ index.

Figure 9 presents the results for the 25 m receiver and the $L_{Aeq,Tp}$ index in the case of the Single Unit trains.

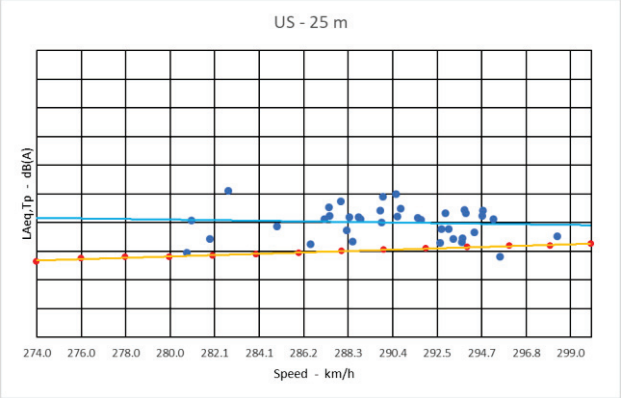

Figure 9: Measured (blue) vs calculated (red) $L_{Aeq,Tp}$ values at 25 m – Single Unit TGV.

The regression line (blue curve) exhibits a negative slope and a standard deviation of 1.1 dB(A). The negative slope shows that train speed is not the only variable parameter influencing the noise level at the receiver. Other factors such as train condition add variability to the measured levels. At 25 m, variations in weather conditions have a small influence. Calculations with the same ground type comparing favorable to homogeneous propagation conditions show a 1 dB(A) difference at 25 m and up to 5 dB(A) at 150 m. Weather conditions monitored during the measurements are not available. Small variations in weather conditions are expected here, despite the fact that all trains were measured within the same day. The calculated $L_{Aeq,Tp}$ values exhibit a regression line (red curve) with a positive slope corresponding to the speed dependence of the sources' emission model. The calculated levels are around 2 dB(A) lower than the measured levels.

Figure 10 presents the same comparison of measured and calculated $L_{Aeq,Tp}$ values obtained for the Multiple Unit trains at 25 m.

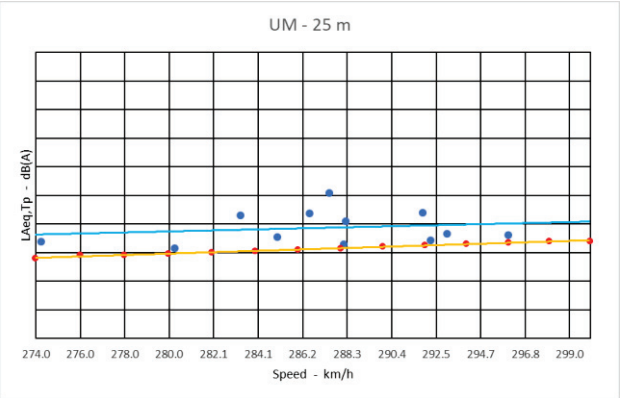

Figure 10: Measured (blue) vs calculated (red) $L_{Aeq,Tp}$ values at 25 m – Multiple Unit TGV.

Similar trends as for the Single Unit trains are observed. The standard deviation of the measured data is 1.1 dB(A). Note that overall, the Multiple Unit trains have $L_{Aeq,Tp}$ values that are very close to the Single Unit trains. This is expected since the track is close to a straight line on each side of the receiver line (see Figure 3).

Now consider the same $L_{Aeq,Tp}$ index for Single Unit trains at the 150 m receiver shown in Figure 11. The measured standard deviation is 3.8 dB(A) in this case. This higher spread is to be expected due to the greater distance which results in increased variability of meteorological effects. It should be noted that the slope of the regression line of the measured data is now positive and close to the slope of the calculated values. Overall, the calculated levels are now about 2 dB(A) greater than the measured values estimated from the regression.

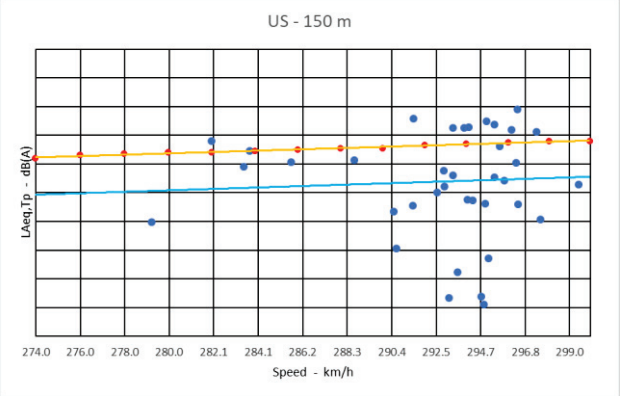

Figure 11: Measured (blue) vs calculated (red) $L_{Aeq,Tp}$ values at 150 m – Single Unit TGV.

Figure 12 present the same comparison for the Multiple Unit trains. Again, similar trends as for the Single Unit trains are observed. The standard deviation of the measured data is 4.2 dB(A).

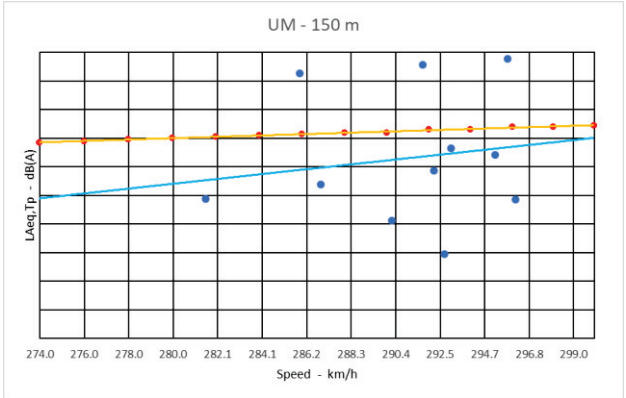

Figure 12: Measured (blue) vs calculated (red) $L_{Aeq,Tp}$ values at 150 m – Multiple Unit TGV.

4.2 Measured and calculated $L_{A,max}$

This section presents the results obtained for the $L_{A,max}$ index.

Figure 13 and Figure 14 show the measured and calculated $L_{A,max,1sec}$ at 25 m for Single Unit and Multiple Unit trains, respectively. The standard deviation for the measured values is 1.4 dB(A) for both cases. As expected, this value is higher than for the $L_{Aeq,Tp}$ due to the fact that the maximum level does not include an averaging process over the pass-by time as in the case of SEL, TEL or $L_{Aeq,Tp}$ indexes. Also, the calculated values are approximately 4 dB(A) below the measurement regression line. This is likely due to the larger standard deviation and the fact that the maximum level is influenced by short variations with potentially high-level peaks in the train acoustic emission. These variations are not taken into account in the source definition and in the calculation, which considers an averaged emission power level. As a result, the calculated $L_{A,max}$ is likely to underestimate or overestimate the measured $L_{A,max}$ especially for sources with non-stationary emission.

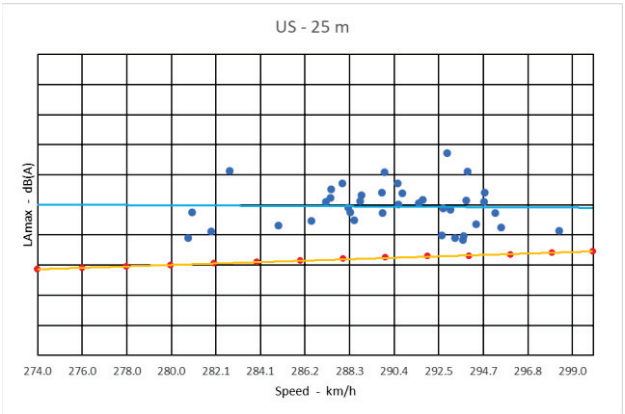

Figure 13. Measured (blue) vs calculated (red) $L_{A,max,1sec}$ values at 25 m – Single Unit TGV.

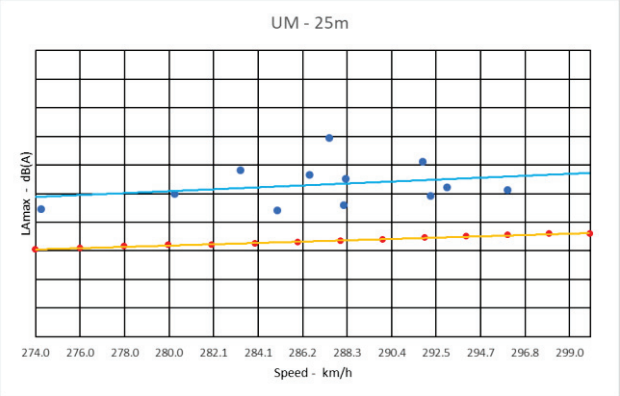

Figure 14. Measured (blue) vs calculated (red) $L_{A,max,1sec}$ values at 25 m – Multiple Unit TGV.

Figure 15 and Figure 16 show the same results at 150 m for Single Unit and Multiple Unit trains, respectively. The standard deviation for the measured values is 3.6 dB(A) for the Single Unit trains and 4.2 dB(A) for the Multiple Unit trains. The calculated values are approximately 1 dB(A) above the measurement regression line for the Single Unit case. For the Multiple Unit case, the slope of the measurement regression line does not follow the calculated slope. Even though, the calculated values seem to better match the measured values than in the case of the $L_{Aeq,Tp}$ index, it is likely that the underestimation visible at 25 m is compensated at 150 m by the slight over-estimation possibly due to weather effects which was already seen in the $L_{Aeq,Tp}$ comparisons (see Figure 11 and Figure 12).

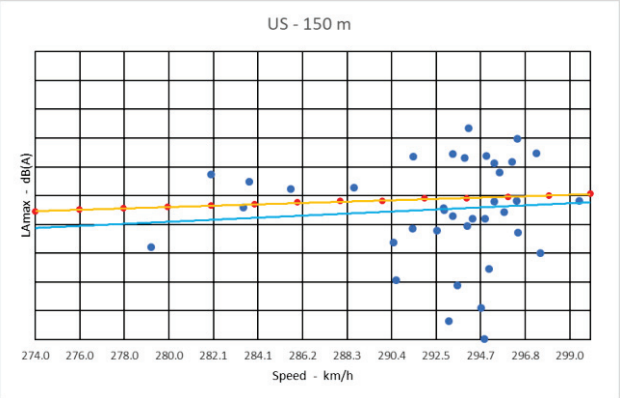

Figure 15. Measured (blue) vs calculated (red) $L_{A,max,1sec}$ values at 150 m – Single Unit TGV.

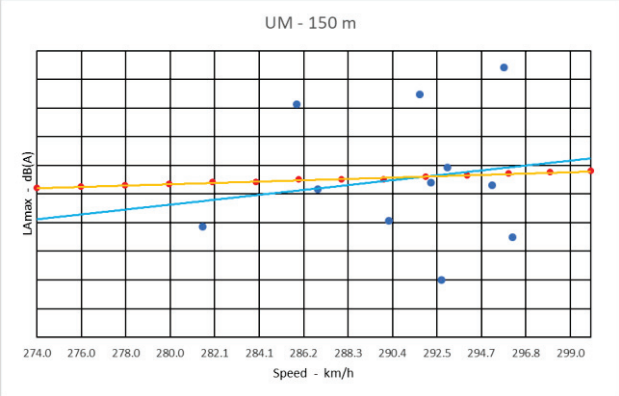

Figure 16. Measured (blue) vs calculated (red) $L_{A,max,1sec}$ values at 150 m – Multiple Unit TGV.

5. CONCLUSIONS

This paper presents a simple method for estimating standard event related short-term indexes such as $L_{Aeq,Tp}$, SEL, TEL and $L_{A,max}$ derived from the time evolution of the instantaneous sound pressure level. The approach is based on the existing engineering calculation methods for outdoor noise propagation and relies on the discretization of the line source in the geometrical calculation phase.

In this preliminary validation study, the calculated values for the $L_{Aeq,Tp}$ and $L_{A,max}$ indexes are compared to measured values obtained for high-speed train pass-by events at two receiver locations, 25 m and 150 m away from the track. The calculations use the French NMPB2008 propagation model and SNCF train sources emission model. Results show an agreement between the calculated and measured mean values within approximately 2 dB(A) for the $L_{Aeq,Tp}$ index and 4 dB(A) for the $L_{A,max}$ index. However, it should also be pointed out that the deterministic source definition and propagation model are unable to reproduce the relatively large variations of this short and very short-term indicators obtained from single pass-by, i.e., unaveraged, measurements.

Future work will first attempt to better explain the differences between measured and calculated mean values by varying parameters such as weather conditions as well as considering other emissions models (such as the CNOSSOS-EU model allowing the modeling of aerodynamic noise sources) and advanced propagation methods (such as the Harmonoise method allowing a finer characterization of ground and meteorological conditions). Also, the approach will be further tested for other types of trains and different site configurations.

6. REFERENCES

[1] L. Fritschi *et al.*: "Burden of disease from environmental noise: Quantification of healthy life years lost in Europe," *World Health Organization Regional Office for Europe (2011)*.

[2] Eze, I.C. *et al.*: "Transportation noise exposure, noise annoyance and respiratory health in adults: A repeated-measures study," *Environment International,* 121, pp. 741-750, 2018.

[3] Schreckenberg, D., Belke, C., Spilski, J.: "The development of a multiple-item annoyance scale (MIAS) for transportation noise annoyance," *International Journal of Environmental Research and Public Health,* 15 (5), art. no. 971, 2018.

[4] Gille, L.-A., Marquis-Favre, C.: "Estimation of field psychoacoustic indices and predictive annoyance models for road traffic noise combined with aircraft noise," *Journal of the Acoustical Society of America, 145 (4), pp. 2294-2304 (2014)*.

[5] Vallin, P.-A., Marquis-Favre, C., Bleuse, J., Gille, L.-A.: "Railway noise annoyance modeling: Accounting for noise sensitivity and different acoustical features," *Journal of the Acoustical Society of America,* 144 (6), (2018).

[6] Di, G.-Q., Lin, Q.-L., Li, Z.-G., & Kang, J. : "Annoyance and activity disturbance induced by high-speed railway and conventional railway noise: a contrastive case study". *Environmental Health (2011).*

[7] Aasvang, G. M., Moum, T., & Engdahl, B.: "A field study of effects of road traffic and railway noise on polysomnographic sleep parameters," *Journal of the Acoustical Society of America*, 129(6), (2011).

[8] Dutilleux G. *et al.*: "NMPB-routes-2008: The revision of the French method for road traffic noise prediction," *Acta Acustica united with Acustica,* 96(3):452–62, 2010.

[9] Van Maercke, D. and Defrance, J.: "Development of an analytical model for outdoor sound propagation within the Harmonoise project," *Acta Acustica united with Acustica,* 93(2):201–212, 2007.

[10] Kephalopoulos, S. *et al.*: "Common noise assessment methods in Europe (CNOSSOS-EU)," *European Commission Joint Research Centre,* 2012.

[11] ISO 3095:2013 "Acoustics - Railway applications - Measurement of noise emitted by railbound vehicles".

[12] Morse, P. M. and Ingard, K. U.: "Theoretical Acoustics," Princeton, NJ, 1986.